Monitoring and failure mechanism interpretation of an unstable slope in Southern Switzerland based on terrestrial laser scanner

Pedrazzini Andrea, Antonio Abellan & Michel Jaboyedoff
Institute of Geomatics and Risk Analysis, Univ. of Lausanne, Switzerland
Thierry Oppikofer
Norwegian Geological Survey, Trondheim, Norway

2011 Pan-Am CGS Geotechnical Conference

ABSTRACT
We present the application of terrestrial laser scanning (TLS) for the monitoring and characterization of an active landslide area in Val Canaria (Ticino, Southern Swiss Alps). At catchment scale, the study area is affected by a large Deep Seated Gravitational Slope Deformation (DSGSD) area presenting, in the lower boundary, several retrogressive landslides active since the 1990s. Due to its frequent landslide events this area was periodically monitored by TLS since 2006. Periodic acquisitions provided new information on 3D displacements at the bottom of slope and the detection of centimetre to decimetre level scale changes (e.g. rockfall and pre-failure deformations). In October 2009, a major slope collapse occured at the bottom of the most unstable area. Based on the comparison between TLS data before and after the collapse, we carried out a detailed failure mechanism analysis and volume calculation.

RÉSUMÉ
Dans cette étude, l'utilisation du scanner laser terrestre pour l'étude des mouvements d'un versant rocheux actif est présentée. Le site d'étude situé en Val Canaria (partie Sud des Alpes Suisses) est caractérisé par la présence d'une zone de tassement de grand ampleur qui présente à son pied plusieurs zones de glissement régressifs particulièrement actives. Un suivi régulier par scanner laser terrestre, effectué depuis 2006, a permis l'analyse très détaillé des mouvements en trois dimensions de l'activité de chute de blocs. En octobre 2009, un important éboulement de 360'000 m^3 est survenu dans la partie inférieure du versant. Les données laser acquises avant et après l'éboulement ont permi une analyse détaillée du mécanisme de rupture et du volume mobilisé.

1 INTRODUCTION

Rockfalls and rockslides represent a major hazard in alpine valleys, especially along transportation corridors and populated areas (Remondo et al., 2008). Nowadays, almost all the alpine countries dispose of scientific studies to characterize rockfall hazard at least in areas where a potential conflict between human activities is present (Lateltin 1997; Raezo et al., 2002). Nevertheless, few studies investigated the indirect risk posed of landslide dam obstructing rivers and lakes in alpine catchment that could leads to downstream flooding (Bonnard, 2011; Eisbacher and Clague, 1984).

In this study, the characteristics of the Val Canaria in terms of type and distribution of slope instabilities will be presented. Firstly, the lithological and tectonic characteristics, influencing the location and type of movement will be analyzed. Secondly, a more detailed study on a potential large collapse located directly above the Canaria River will be presented.

This area represents a potential hazard to the village and the highway situated at the bottom of Val Canaria: Large rock collapse may create landslide dams in the narrow valley that could fail catastrophically and create an important downstream flooding.

In this area, periodic Terrestrial Laser Scanning (TLS) acquisitions were carried out since 2006 aiming to characterize the instability in terms of structures and potential pre-failure displacements. In October 2009, an important rock collapse occurred on the monitored area. TLS datasets acquired the day before and the days after the event allowed the detection of pre-failure movements and the computation of the collapsed volume. Based on this information, an interpretation of main predisposing and triggering factors leading to the failure is proposed.

The complex geological setting of Val Canaria represents also an interesting study area, where the type and the distribution of slope movements are clearly linked to tectonic and lithological characteristics. Detailed study of the relationship between lithology, tectonics and slope movements could also improve the understanding in term potential hazard posed by the different type of instabilities.

2 STUDY AREA

The study area is located in the Gotthard area, near the village of Airolo (southern Switzerland). Val Canaria is a lateral NE-SW valley (Figure 1). This 18 km^2-large catchment presents elevations ranging from 1100 m to 2700 m with mean annual rainfalls of about 1400 mm.

The area is historically well known for its susceptibility to slope instabilities since more than 150 years. According to Baruffini and Ambrosi (2010), an important rock collapse occurred in the southern part of the valley in 1846. Furthermore, a landslide located in the north-western flank of the valley was reactivated in spring 1992, after a rapid snow melting. This event created a temporarily landslide dam obstructing the Canaria River (Seno and Thüring, 2006).

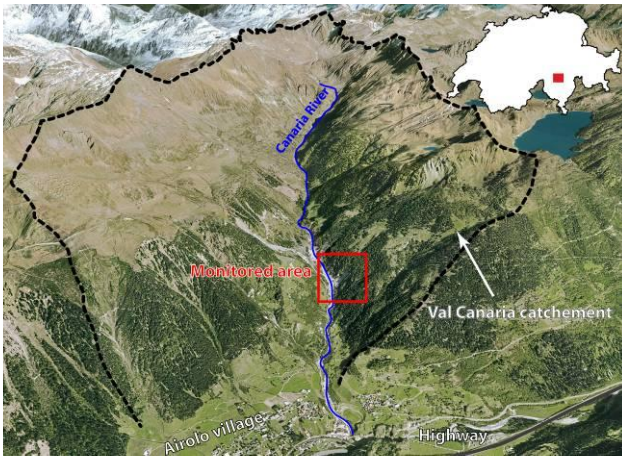

Figure 1: 3D view toward north of the Val Canaria catchment showing the TLS monitored area (red rectangle).

Val Canaria is dominated by the Mesozoic autochthonous cover of the Gotthard massif. The area is tectonically complex due to the presence of a large syncline (Piora syncline) that folds the meta-sediments covering the Gotthard massif. The outcropping lithologies are: (a) gypsum and dolomitic breccia in the lower part of the valley, (b) calc-schist in the eastern and in the central part of the valley; (c) orthogneiss and granite belonging to the Gotthard basement in the north-western flank of the valley (Figure 3).

3 METHODOLOGY

3.1 Instability mapping at catchment scale

The first task of this study was to identify the main rock slope instabilities presented in the area. Digital support like orthophotos, a 10 m cell size digital elevation model (DEM), geological maps and Google Earth™ have been used for the first detection. Available literature on the previously known instabilities was also consulted and integrated in the mapping task (Seno and Thüring, 2006, Antognini al., 1996).

3.2 Terrestrial laser scanner monitoring

The lower part of most active landslide of Val Canaria has been surveyed using an Optech ILRIS3D. Distance measurement is based on the time-of-flight of the laser pulse, i.e. the time to travel and reflect from the rock surface. Maximum operational range of the ILRIS3D is around 700 m. TLS accuracy supplied by the manufacture is 7 mm at a distance of 100 m. More detailed information about TLS methodology and applications can be found in Rosser et al. (2007), Teza et al. (2007), Abellan et al. (2009) and Oppikofer et al. (2009).

3.2.1 Data acquisition

Eight TLS surveys were acquired between June 2006 and October 2010. The rock slope was scanned from 4 different positions in order to completely cover the area. The mean point spacing on the rock face, depends on the site configuration and distances to the TLS, and ranges between 5 to 12 cm. After vegetation cleaning, each dataset contained between 4 and 7 million points.

3.2.2 Co-registration of the point cloud

TLS datasets acquired during the same campaign were co-registered in a single point cloud using PolyWorks software (InnovMetrics). Merged scans were preliminary aligned using common points (N point pairs). A refinement of the alignment was carried out using Iterative Closest Point (ICP) algorithm (Chen and Medioni, 1992). Co-registration error could be estimated to 2.8 cm.

3.2.3 Displacements characterization and quantification

Two different methods have been applied in order to characterize and quantify the displacements:

- Point to surface comparison: Shortest Distances (SD) between the reference point cloud and the successive datasets (Oppikofer et al., 2008; 2009).
- Roto-translation matrix technique (Monserrat and Crosetto, 2008; Oppikofer et al., 2009)

As suggested by Oppikofer et al., (2009), SD analysis is a useful tool to detected 3D displacement allowing the identification of vertical, horizontal and oblique differences. The computation of SD was performed in PolyWorks software. For each point of a data point cloud the SD algorithm searches its nearest neighbour in the reference point could and computes the SD vector. Regarding sign criteria, positive SD indicate that the points in the data point cloud are situated above the reference point cloud (sliding mass advance from its initial position). Negative SD means that the data point cloud is behind or below the reference dataset. Negative SD could be interpreted as vertical settlement, subsidence or rockfalls (Oppikofer et al., 2008; 2009). The advantage of this method is the quick application that could be performed automatically to detect movements between the reference and the successive datasets. The main disadvantage is that SD analysis is performed for point pairs only. This implies that the quality of comparison results depends strongly on the point spacing and on the presence of shadow zones. In addition, the comparison must be ideally performed between datasets acquired almost from the same position. As suggested by Oppikofer et al. (2009) the error associated with the SD comparison cloud be estimated as the standard deviation obtained during the registration of sequential datasets, which is approximately 2.5 cm in this study.
To assess smaller displacements and to compare datasets acquired from slightly different positions the roto-translation matrix technique was applied. This method account for both translation and rotation of a selected area (e.g. rock slope compartment, block, portion of soil), considering all the data points. As suggested by Oppikofer et al. (2009) translation of the central point of the selected area could be expressed by trend, plunge and vector norm. The rotation is expressed

by the toppling azimuth and angle of an initially vertical vector and the tilt rotation around the toppled vector. The methodology is described in detail in Oppikofer et al. (2009). Compared to the SD analysis, the roto-translation matrix technique presents a great advantage by using the high point density of TLS data to estimate mean displacements of a selected area. Using this method, displacements of approximately 1 cm can be detected. Main limitations of this technique are related to the detection of homogenous areas that could display constant deformation behaviour.

3.2.4 Volume estimation

In order to estimate rockfall and rockslide volume, we created DEMs from the TLS point clouds of the reference dataset and the successive acquisitions. Inverse distance weighted (IDW) interpolation was applied to create 0.2 m cell size DEMs. Failed volumes correspond to the sum of the differences between successive DEMs over the collapsed area.

3.2.5 Structural analyses

According to Brideau et al., (2009), structural analysis is one of the most important steps for the definition of the potential failure mechanism on hard-rock slopes. In this study, we obtained the orientation of the main discontinuity sets on the base of TLS data using COLTOP3D software (Jaboyedoff et al., 2007). This software allows computing the spatial orientation (dip direction and dip angle) of each point with respect to its neighbourhood. An interactive selection of different orientations is possible, allowing a user-friendly exportation of the discontinuity orientation to common stereographic software (e.g. Dips). Main advantage of this technique is the possibility to obtain a quick and visual identification of the main orientation based on an orientation-specific colouring of the point cloud. This technique is relatively quick compared to manual techniques (Sturzenegger and Stead, 2009) and allows obtaining a large amount of structural data giving a more complete statistical description of the natural variability of different discontinuity sets.

4 RESULTS (1): INSTABILITY CHARACTERIZATION AT CATCHMENT SCALE

Photo-interpretation allowed for the identification and mapping of more than 30 slope instabilities affecting the Val Canaria catchment at different scales. 55% of the entire catchment is exposed to gravitational movements. We observed that the location and activity of the slope instabilities along the valley were not homogenously distributed (Figure 2). The most important slope destabilizations are concentrated in the lower part of the valley. In this area, both valley flanks are characterized by deep seated deformations and by several more superficial instabilities. A clear distinction between the geomorphological features characterizing the two valley flanks is shown in Figure 3, as follows: (a) the upper part of the NW flank is characterized by a massif presence of large trenches and counter-scarp features. However, the present–day active scarps are located in the lower part; (b) in the SE flank no counter scraps were observed. The topography is rough but the slope is quite uniform along the slope. In the lower portion of the slope close to the river, a series of active scars were observed.

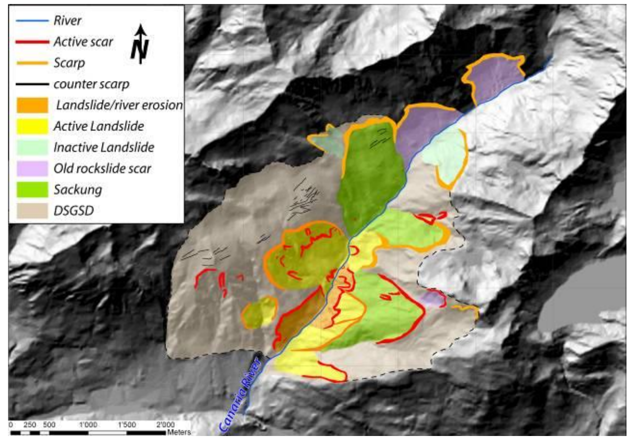

Figure 2: Map of the different slope instabilities detected through DEM and aerial photos analysis.

By analysing the distribution of slope instabilities in relation to tectonic features, it is possible to observe that the most active area corresponds to the lower part of the valley, where gypsum outcrops. In this area, the valley is sub-parallel to the Piora syncline axis. The presence of gypsum at the bottom of the slope represents a major destabilizing factor that was pointed out by several authors working in the Alpine area (Alberto et al., 2008; Dramis and Sorriso-Valvo, 1994). Dissolution of gypsum at the bottom of the slope favours the creation of large slope instabilities as deep seated creeping observed in both flanks of the valley. Typology and the style of activity are also influenced by tectonic heritage. Instabilities could be described as large collapse and sliding in the south-eastern portion of valley. This is probably related to low rock mass strength of the lithology outcropping in the area and to the bedding attitude sub-parallel to slope direction. The NW flank of the valley shows the opposite situation with the main foliation of high strength orthogneiss dipping into the slope. This geological configuration induces the creation of compressional features, such as counter-scarps and trenches in the upper part of the slope (Figure 3). Gypsum dissolution at the bottom of the slope allows the development of large slope creeping. Slope activity decreases progressively in the more internal part of the catchment where the Piora syncline and its related soluble rocks are not parallel to the valley. The outcrops are mainly massive orthogneiss with the main foliation orientated orthogonally to the slope orientation, which is less prone to slope instabilities.

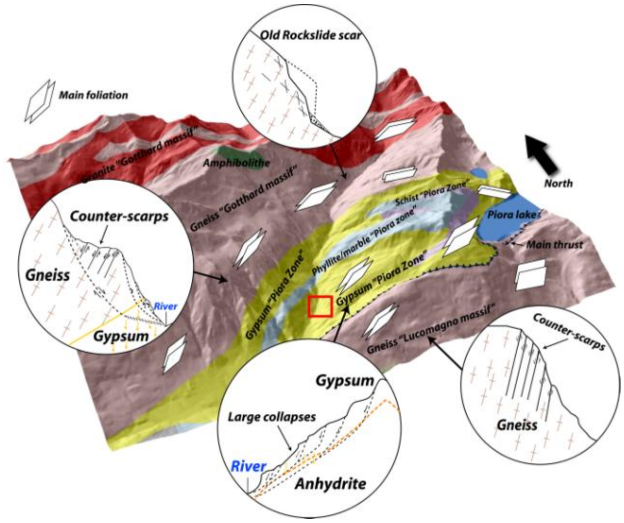

Figure 3: 3D sketch of the tectonic settings of the Canaria catchment, including the main instability types based on the foliation orientation and the lithological characteristics.

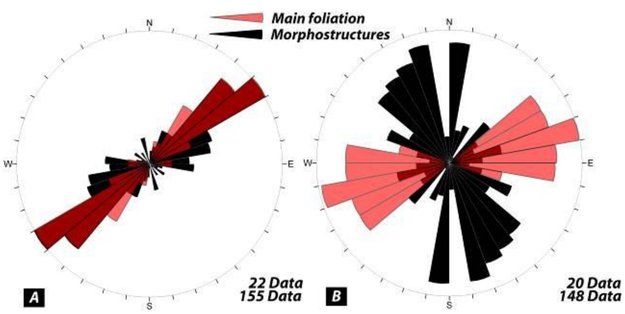

Figure 4: Comparison between bedding attitude and morphostructures in the (a) NW valley flank and (b) in the SE flank, showing a clear distinction of structural and lithological control between the two valley flanks.

5 RESULTS (2): LOCAL KINEMATIC ANALYSIS

At the bottom of the SE flank of valley an active scar formed on gypsum outcrop could be underlined (Figure 5). The area shows an increasing activity since the 1990s. Due to its proximity to the Canaria River and the possibility to create a landslide dam the area is monitored using total station techniques (Ambrosi, pers. comm.). Rockfall activity is frequently observed especially during melting periods and after rainfall events. In the past, the area experienced important rock collapse involving 10'000 m^3 of weathered gypsum.

5.1 Structural setting

A detailed structural analysis was carried out on TLS data acquired prior and after the 27 October 2009 landslide. Due to the gypsum mechanical behavior, development of discontinuity sets is frequently scattered. Failure occurs commonly by rock mass collapse. However, field observations indicate that large structures are found also in gypsum and could influence the failure mechanism. By using the two TLS, it was possible to obtain a double control of the meaningfulness of the detected structures.

Figure 5: Picture showing the evolution of the monitored area between the 2006 and 2009.

Using COLTOP3D analysis, 6 discontinuity sets and the bedding planes were detected on both datasets with very similar values (Table 1 and Figure 6a to c). A kinematic analysis was conducted for the average topography of the cliff in order to detect the main potential failure mechanisms. Results indicated that planar sliding is locally possible along S0. Along intersections J4/J6, J7/S0, J7/J6 and S0/J4 wedge sliding is kinematically feasible and is marginally feasible along J7/J2 and J6/S0. Due to the high variability of discontinuity J3, toppling on this discontinuity is also locally possible. Rock instabilities in moderate to low rock mass qualities (e.g. gypsum, dolomitic breccia) are mainly controlled by rock mass strength (Brideau et al., 2009).

Table 1: Main discontinuity sets detected on TLS point clouds acquired before and after the 27 October rockslide.

Joint set	TLS 2007	Variability 1σ/2σ	TLS 2010	Spacing (m)	Variability 1σ/2σ
J1	178/72	11/18	172/69	2	12/19
J2	059/71	12/21	54/73	1.5	7/12
J3	153/64	12/20	153/64	2	12/20
J4	216/68	7/12	230/61	1	10/17
S0	341/55	14/23	324/69	0.2	9/16
J6	023/68	11/19	023/73	0.5	11/19
J7	260/60	10/17	266/54	0.5	11/18

Nevertheless, rock mass anisotropy related to the presence of one direction of fracturing or to a preferential fracturing direction could reduce the strength in a preferential direction (Amadei and Savage, 1989). For this reason, the direction of the maximum discontinuity frequency (Hudson and Priest, 1983; Jaboyedoff et al., 1995) has been analyzed in order to investigate the possible relationship between structural setting, potential strength anisotropy and the topography orientation (Figure 6d). Results indicate that the maximum discontinuity frequency direction (63° toward 340) defines a surface close to the mean orientation of the rockslide slope (300/55). This result pointed out that the surface of the scarp is not fully controlled by one distinct discontinuity set (i.e. beddings) or only by glacial or fluvial erosion but by the combination of discontinuity sets. Highest density direction calculated form of pre-existing discontinuities needs to be considered as important influence on slope orientation and failure direction.

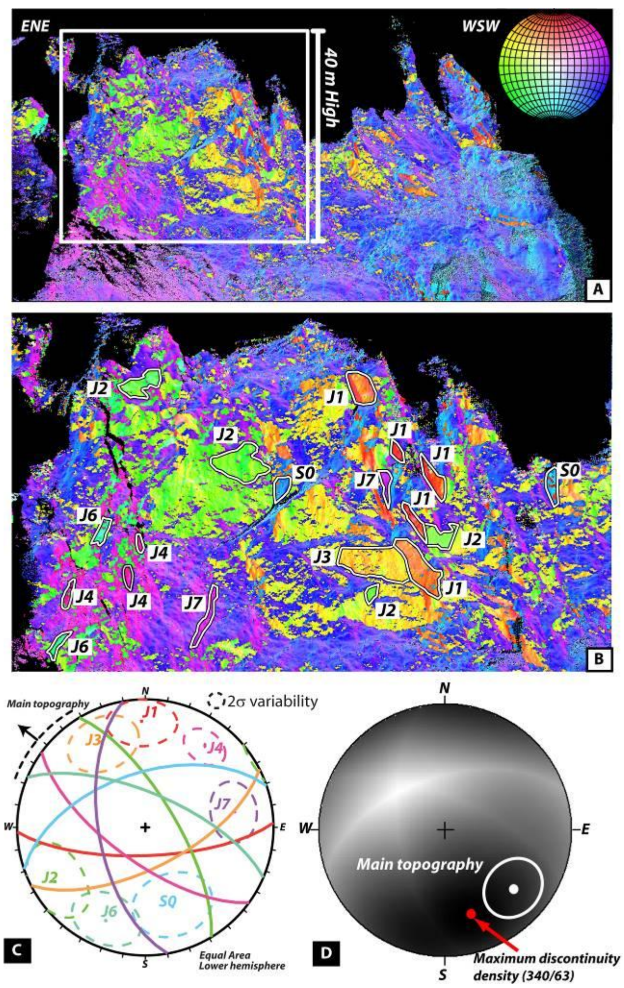

Figure 6: A) COLTOP3D representation of 2007 TLS dataset. B) Zoom showing the selected discontinuity set. C) Stereographic projection of discontinuity set detected on 2007 TLS dataset. D) Direction of the maximal discontinuity density obtained by coupling all the detected discontinuity sets and compared to the local topography orientation.

6 RESULTS (3): EVOLUTION OF THE MONITORED AREA DURING TIME

The activity of the area was evaluated by comparing the different TLS data acquired between 2006 and 2010. The comparison was carried out dividing the observation period in three different time spans, corresponding to pre, syn and post failure period. These three time spans will be analyzed separately.

6.1 Time span 1: datasets acquired in 2006, 2007 and 2009.

We used the SD analysis to compare the TLS datasets acquired in 2006 (reference dataset) to scans acquired in 2007 and 2009 (26.10.2009). Displacement analysis between the first two datasets (2006 and 2007) reveals significant rock collapse in the WSW sector (Figure 7a) of the slope and pre-failure displacements, up to 15 cm in the central part of the rock mass (Figure 7b). Debris movements as well as material deposition are observed in the lower portion of the slope. Point cloud comparison between 2007 and 2009 shows an increasing displacement rate in the central part of the slope with movement that reach locally more than 1m in 2 years. The SW part of the slope shows smaller rock collapses.

The rock outcrops were divided into six blocks based on the morphology and differential displacements observed based on SD technique for a detailed 3D displacement analysis using the roto-translation matrix technique. This procedure ensures that the computed translational and rotational displacements of the blocks are representative for each analyzed zones. In order to assess the errors with the given datasets, five areas that were assumed stable in the surroundings of the moving area were used as reference blocks. Analyses on reference blocks indicate an accuracy of the translation length varying between 0.02 and 2.41 cm with an average of 1.20 cm. The error on rotational components ranges from 0.008° to 0.227° with a mean value of 0.068° for the toppling angle and from 0.002° to 0.104° with an average of 0.041° for the tilt angle.

Translation vectors have a relatively constant trend and plunge (average of blocks between 2006 and 2009: 292°/34°) with only little variations between the different blocks (trend: [284°; 327°]; plunge: [24°; 51°] and the different epochs (1σ standard deviation between displacement vector orientations: mean: 11.4°; max: 22.4°). The translation velocity between 2007 and 2009 [22.9 cm/year; 50.8 cm/year] are 2.5 to 4 times higher than between 2006 and 2007 corresponding to 8.2 cm/year; 17.9 cm/year respectively. Most measured toppling angles are significant, although their accuracy is relatively low (mean error of reference blocks: 0.068°). Toppling angles vary between 0.011° and 0.382° and the toppling directions range from 210° to 037°, i.e. principally in down slope direction. Average toppling is 0.176°/year towards 301°N. For blocks that had significant toppling between 2006 and 2007, the annual toppling angle is slightly higher in the successive period between 2007 and 2009.

6.1.1 Movements interpretation

TLS analysis indicates an increase of the movement of the central part of the slope between 2007 and 2009.
The entire rock mass seems to be moving almost in the same direction, indicating that the frontal block is not completely disconnected from the entire rock mass. Displacement directions appear to be controlled by the structural settings: COLTOP3D analyses underline the presence of at least three potential wedges (S0/J4, S0/J7 and J6/J7) with similar trend and plunge as the observed movements. Blocks located in the WSW part of the slope show faster movements than blocks analyzed in the ESE part. The WSW part of the rock slope experienced a large slope collapse between 2006 and 2007 that was estimated between 12'500 and 13'000 m^3 based on TLS comparison. A possible explanation of this collapse could be related to the concave topography allowing a water concentration inducing a drastic decrease of the effective rock mass strength. This explanation is also supported by measured tilt angles indicating a clockwise rotational movement for all monitored blocks.

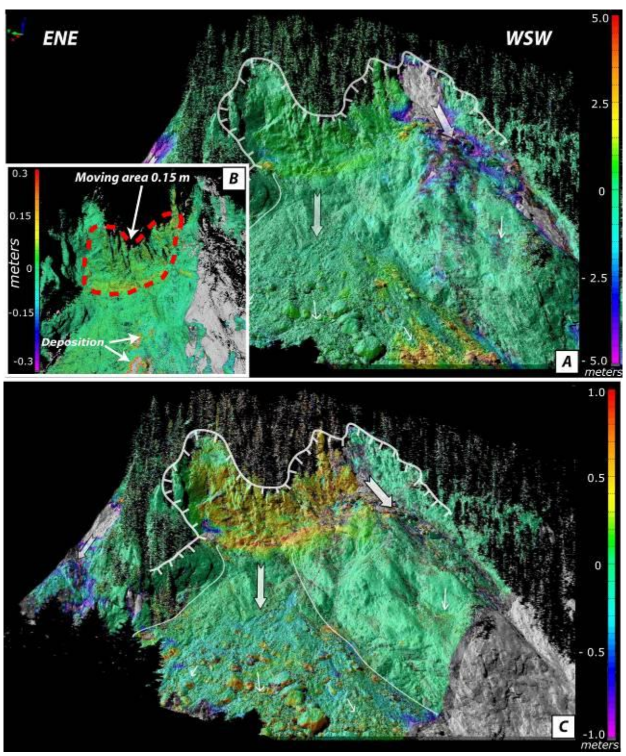

Figure 7: SD comparison between 2006, 2007 and 2009. A) SD comparison (+/- 5m) between 2006 and 2007 showing the rockfall that occurred in the WSW part of the rock cliff. B) SD comparison of the same period (+/- 0.3 m) highlighting uniform displacements of the entire central part of the slope. C) Displacements in the central part of the slope between 2007 and 2009.

6.2 Time span 2: Comparison of scans acquired the day before the main rockslide event (26.10.2009).

A complete TLS campaign of the unstable zone was conducted one day before the main rockslide event that completely changed the topography of the area.
The area was scanned almost from the same position, in the morning (11.40 AM) and at the end of the afternoon (5.30 PM). SD analysis was applied to compare TLS datasets acquired in the morning (reference dataset) to scans acquired afternoon. This displacement analysis does not reveal significant differences, i.e. larger than the co-registration errors ($1\sigma = 2.8$ cm). The roto-translation matrix technique has been applied to the same compartments as in the 2006-2009 analysis. Two areas located in the lower part of the slope were assumed stable and were used as reference blocks (Figure 8). The calculated error for translation (vector norm) varies between 0.5 and 0.95 cm and average errors for the rotational components reach 0.05° for the toppling angle and 0.04° for the tilt angle.
The ENE portion of the slope, translation vectors have a similar length (1.7 and 1.8 cm for Block 1 and Block 2 respectively) and both blocks slide in the slope direction, but with different plunge angles. Block 3 located in the western part of the slope, shows a more important vector norm of about 2.9 cm with a direction plunging into the slope. Toppling and tilt angles are not significant with respect to the errors measured on the stable parts.

6.2.1 Movements interpretation

The interpretation of the deformation is difficult because the measured movements are close to the limits of accuracy of the roto-translation matrix method. The measured translation displacements can be compared to ground-based radar measurements acquired the same day between 12.00 AM and 3.15 PM. The radar survey showed mean displacements of about 0.65 cm for the entire central part (Strozzi T., Pers. Comm.). The agreement is good, considering that the displacement measured by the radar are related only to the line of sight and that the observation period (3:15 hours) is shorter than the time laps between the two TLS acquisition (5:15 hours). The differences in plunge angle of Blocks 1 and 2 could be related to the important fracturing and block individualization preceding the main collapse, which occurred 12 hours after the last TLS acquisition. During this phase, displacements of the rock mass could show different movement patterns. Block 3 shows a displacement direction pointing into the slope. These results are not surprising considering that block 3 is almost completely detached form the main rock cliff by a persistent fracture probably acting as strike-slip fault, allowing Block 3 to sag and to rotate. This corresponds, in the roto-translation matrix analysis, to a vector plunging in to the slope.

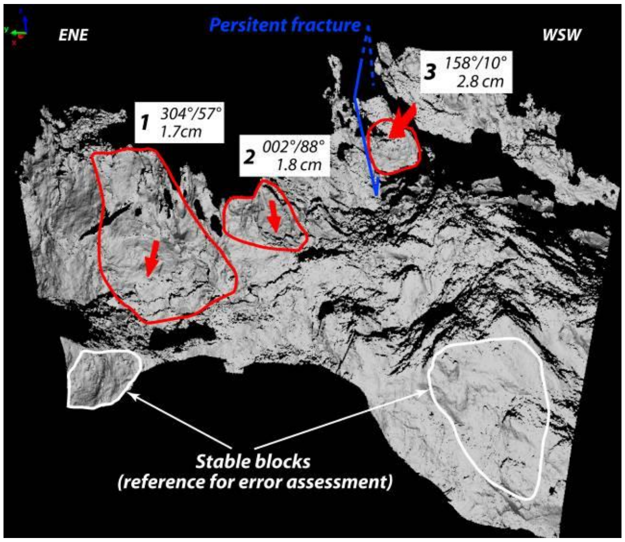

Figure 8: Results of roto-translation matrix technique applied to TLS dataset acquired the day before the rockslide event (26 October 2009).

6.3 Time span 3: Comparison between scan taken after the main rockslide event (29.10.2009-28.10.2010).

After the main rockslide event, five TLS datasets were acquired in order to follow the slope evolution after the rockslide event. SD comparison of TLS data the entire period (29.10 2009 vs. 28.10.2010) indicates an important displacement of the upper portion of the debris cone (up to 5 m) toward the valley bottom (Figure 9). The ENE part of the rockslide scar shows important differential movement of up to 15 cm (Figure 9). This indicates that new large instabilities could develop in the ENE part of the slope. In the same area, an important rockfall activity was observed all along the post failure period. The volume of the observed rockfalls progressively decreases from the early to the last TLS acquisition. In the first observation period (October - November 2009) detected rockfalls have a maximum volume of 5 m^3. In the following period the volumes decreases to maximum 1 m^3 for singular events.

7 RESULTS (4): CHARACTERIZATION OF THE OCTOBER 2009 ROCKSLIDE

The quantification of the failed volume was carried out by DEM differences derived from TLS point clouds. Results indicate a failed volume of 365'000 m^3 and the deposits are estimated to 430'000 m^3 (Figure 10). Differences between the two calculated volumes represent a swelling factor of 15-18%. The error on the volume calculation appear to be mainly related to the presence of shadow zones in the TLS datasets and to the interpolation of 3D point clouds and could be estimated as +/- 10 % for both source and deposition volumes. The run-out length is about 316 m and the height difference is around 250 m correspond to a fahrböschung angle of 35-36°. Pre-failure movements observed in the frontal part of the instability were fairly uniform following a NW direction.

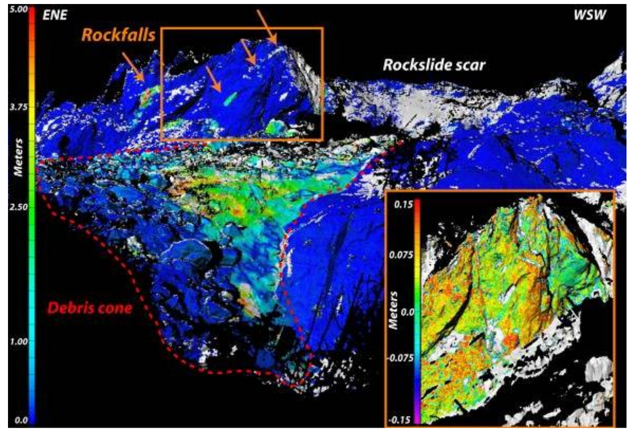

Figure 9: SD comparison between TLS data acquired in November 2009 and October 2010 showing the rockfall activity of the ENE sector of the slope. Zoom of the same area indicates post-failure displacements of about 10-15 cm of the most external block forming the rock mass.

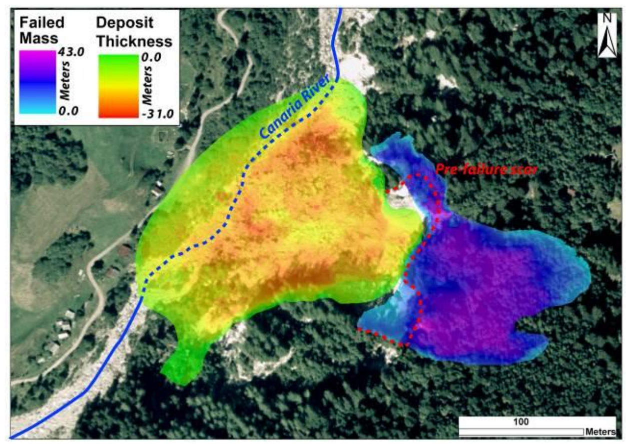

Figure 10: Map of deposit and failed mass thickness based on TLS DEM taken before and after the 27.10.2009 rockslide event. The DEM have a cell size of 20 cm.

Structural analysis indicates the possibility to have several wedges plunging in the same direction. Based on the structural setting, the movement may be explained by a retrogressive sliding/collapse driven by wedge intersection line S0/J4, S0/J7 or J6/J7 and by the progressive degradation of the gypsum, especially along the direction of the maximum discontinuity frequency. Based on the present-day scar morphology, the rear release surface seems to be controlled by J1 and J3. The depth of the failure surface is controlled by the change of rock mass properties at the limit between weathered gypsum and fresh anhydrite. Based on borehole data located close to the rockslide area, the lithological change is located between 45 and 56 meters (Gassman et al., 1979). This depth corresponds quite well to the depth of the failure surface estimated by differences in DEM before and after the collapse. The topography of the surrounding area could also be pointed out as a potential predisposing factor for instabilities development. Above the main rock scarp, the topography is mainly concave allowing concentration of superficial and ground water behind the main rock face increasing pore pressure during rainfall.

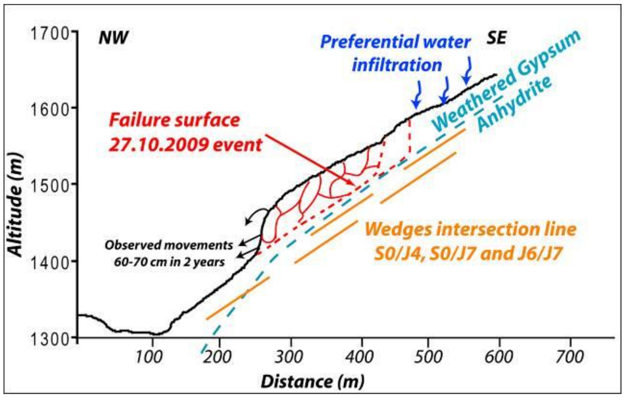

Figure 11: Schematic cross-section showing the structural and geological constraints on the 27.10.2009 rockslide. The failure surface depth is controlled by the changing of rock mass properties between gypsum and anhydrite.

Identification of potential triggering factors are difficult to assess without disposing quantitative data about ground-water level. Based on evidences of other monitored instabilities in the area (Seno and Thüring, 2006) snow melting and rainfall associated to freeze and thaw cycles seem to be the main triggering factors. No seismic event has been registered before the event, so a potential triggering factor could be related to the precipitations occurring during the week before the landslide failure in combination with three days with minimal temperatures below zero before the rockslide.

8 CONCLUSIONS

The Val Canaria catchment shows an important slope activity that could be related to its complex geological settings and tectonic situation. Field evidences indicate different failure mechanisms in the two flanks of the valley. Local analyses based on periodic TLS monitoring allow creating a detailed geological model of the monitored area and an accurate description of pre-failure movements. The structural analysis based on TLS data indicated that discontinuity sets have an important influence on the main movement patterns, even in those lithologies that commonly do not exhibit a structurally controlled failure mechanism. A detailed geometrical characterization of the 27.10.2009 rockslide was carried out based on TLS datasets acquired before and after the event. Coupling structural analysis and pre-failure movement, we proposed a possible failure mechanism corresponding to retrogressive sliding collapse driven by persistent wedge intersection lines and progressive decrease of the rock mass strength related to gypsum dissolution. Long-term displacements and continuous rockfall activity in the area is probably related with the Sackung affecting the entire area.

ACKNOWLEDGEMENTS

The research was supported by Swiss National Foundation (grant number 200021-118105).

REFERENCES

Abellán, A., Jaboyedoff, M., Oppikofer, T., Vilaplana, J. M., 2009. Detection of millimetric deformation using a terrestrial laser scanner: experiment and application to a rockfall event, Nat. Hazards Earth Syst. Sci., 9, 365-372.

Alberto W., Giardino M., Martinotti G., Tiranti D., Geomorphological hazards related to deep dissolution phenomena in the Western Italian Alps: Distribution, assessment and interaction with human activities, *Engineering Geology*, Volume 99, Issues 3-4

Amadei B., Savage W.Z. 1989. Anisotropic Nature of Jointed Rock Mass Strength, *Journal of Engineering Mechanics,* 115, 3, 525-542.

Antognini, M.; Beffa, F.; Valenti, G. 1996. Le glissement de Rutan dei Sassi, Val Canaria (Tessin, Suisse). In: *Bull. angew. Geologie*, vol. 1, Nr. 1, pp. 55-64. Abb., Karten. N1363

Baruffini M, and Ambrosi C. 2010. A GIS-tool for risk assessment due to natural hazards in mountain regions. An exploratory study on an hypothetical event: the Val Canaria flood. Abstract Volume, 8th Swiss Geoscience Meeting.

Bonnard C. Technical and human aspects of historic rockslide dammed lakes and landslide dam breaches. In *Natural and Artificial Rockslide Dams,* Evans, S.G.; Hermanns, R.L.; Strom, A.; Scarascia-Mugnozza, G. (Eds.), Lecture Notes in Earth Sciences, Vol. 133. 570p.

Brideau, M-A., Ming Y., Stead, D. 2009.The role of tectonic damage and brittle rock fracture in the development of large rock slope failure. *Geomorphology*, 103, 30-49.

Chen, Y., Medioni, G., 1992. Object Modelling by Registration of Multiple Range Images. Image and Vision Computing 10, 145–155.

Dramis, F., Sorriso-Valvo, M., 1994. Deep-seated gravitational slope deformations, related landslides and tectonics. *Engineering Geology*. 38, 231/243.

Eisbacher, G.H, and Clauge J.J. 1984. Destructive mass movements in high mountains: Hazard and management, Energy, Mines and Resources Canada (Ottawa)

Gassman J., Gysel M., Schnider J.F.Anhydrit als wirtgestein für die endlangernung radioaktiver Abfälle in der Schweiz. Technische Berich 12, Nagra.

InnovMetric: PolyWorks: 3-D scanner and 3-D digitizer software from InnovMetric Software Inc., http://www.innovmetric.com/Manufacturing/home.aspx , access: February 10, 2011.

Jaboyedoff M., Metzger R., Oppikofer T., Couture R., Derron M.H., Locat J., Durmel D., 2007. New insight techniques to analyze rock-slope relief using DEM and 3D-imaging clouds points : COLTOP-3D software. In: Eberhardt E, Stead D, Morrison T (ed): Rock mechanics: Meeting Society’s Challenges and Demands, Taylor and Francis, 2:61-68

Lateltin, O. 199: Prise en compte des dangers dus aux mouvements de terrain dans le cadre des activités de l’aménagement du territoire, Recommandations, OFEFP, 7.

Monserrat O, Crosetto M. 2008. Deformation measurement using terrestrial laser scanning data and least squares 3D surface matching. ISPRS Journal of Photogrammetry and Remote Sensing 63:142-154.

Oppikofer T., Jaboyedoff M., Blikra L., Derron M.-H and Metzger R. 2009. Characterization and monitoring of the Åknes rockslide using terrestrial laser scanning, *Nat. Hazards Earth Syst. Sci*., 9, 1003-1019.

Oppikofer, T., Jaboyedoff, M. and Keusen, H.-R. 2008. Collapse at the eastern Eiger flank in the Swiss Alps, *Nat. Geosci.* 1, 531-535. doi:10.1038/ngeo258.

Remondo, J., Bonachea, J., and Cendrero, A. 2008. Quantitative landslide risk assessment and mapping on the basis of recent occurrences, *Geomorphology*, 94, 496–507.

Raetzo, H., Lateltin, O., Bollinger, D., and Tripet, J. P. 2002. Hazard assessment in Switzerland – Code of practice for mass movements, Bull. Eng. Geol. Env., 61, 263–268

Rosser, N.J., Lim, N, Petley, D.N., Dunning, S., Allison, R.J., 2007. Patterns of precursory rockfall prior to slope failure. *Journal of Geophysical Research*, Vol. 112, No. F4, doi:10.1029/2006JF000642.

Seno, S., Thüring, M., 2006: Large landslides in Ticino, Southern Switzerland: Geometry and kinematics. *Engineering Geology*, 83, 109-119.

Sturzenegger, M. and Stead, D. 2009. Quantifying discontinuity orientation and persistence on high mountain rock slopes and large landslides using terrestrial remote sensing techniques. *Nat. Hazards Earth Syst. Sci.* 9, 267-287. doi:10.5194/nhess-9-267-2009.

Teza, G., Galgaro, A., Zaltron, N., and Genevois, R.: Terrestrial laser scanner to detect landslide displacement fields: a new approach, Int. J. Remote Sens., 28(16), 3425–3446, 2007.